Molecular Recognition

DOI: 10.1002/anie.201205113

Similar but Different: Thermodynamic and Structural Characterization of a Pair of Enantiomers Binding to Acetylcholinesterase**

Lotta Berg, Moritz S. Niemiec, Weixing Qian, C. David Andersson, Pernilla Wittung-Stafshede, Fredrik Ekström, and Anna Linusson**

In a previous high-throughput screening campaign, we identified the racemate C5685 (**1**) as an inhibitor of *Homo sapiens* acetylcholinesteraste (*h*AChE, Figure 1).[1] Structural analysis of the complex formed between **1** and *Mus musculus* AChE (*m*AChE) revealed that the substituted phenyl ring interacts with the peripheral anionic site (PAS) of *m*AChE, and that the chiral *N*-ethylpyrrolidine moiety of **1** is directed towards the catalytic site (CAS). However, owing to a disordered electron density map we were unable to model the part of **1** that binds to CAS. Furthermore, the electron density map of the side chain of Tyr337 indicated two conformers. These results prompted us to prepare enantiomerically pure **1** and characterize both enantiomers at the kinetic, thermodynamic, and structural levels, as reported herein.

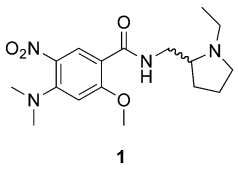

1

Figure 1. The chemical structure of **1** identified as an inhibitor of *h*AChE with a half-maximal inhibitory concentration (IC_{50}) of 1.3 μM.

The synthesis of the enantiomers started with deacetylation of **2**,[2] followed by N-methylation to transform **3** into **4** (Scheme 1).[3] An ester hydrolysis gave the benzoic acid derivative **5**, which was further transformed into the acid chloride and subsequently reacted with (*R*)- or (*S*)-2-(aminomethyl)-1-ethylpyrrolidine to give enantiomerically pure (*R*)-C5685 (**(*R*)-6**) and (*S*)-C5685 (**(*S*)-6**), respectively.

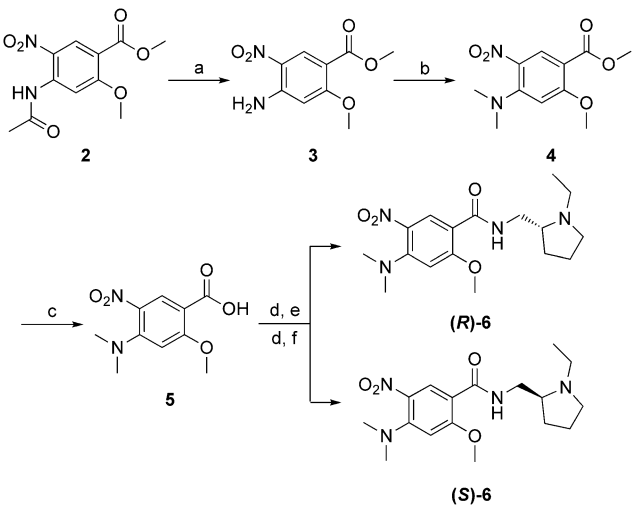

Scheme 1. Synthesis of **(*R*)-6** and **(*S*)-6**. a) MeOH, H_2SO_4, reflux, 96%; b) MeI, NaH, DMSO, RT, quantitative; c) NaOH, dioxane, 55 °C, 93%; d) $(COCl)_2$, DMF, MeCN, 0 °C→RT; e) (*R*)-2-aminomethyl-1-ethylpyrrolidine, Et_3N, CH_2Cl_2, RT, 72% over two steps; f) (*S*)-2-aminomethyl-1-ethylpyrrolidine, Et_3N, CH_2Cl_2, RT, 74% over two steps.

The two enantiomers have nearly identical dose–response relationships with *h*AChE and *m*AChE (Figure 2 and Table 1); this result was unexpected, since previous studies

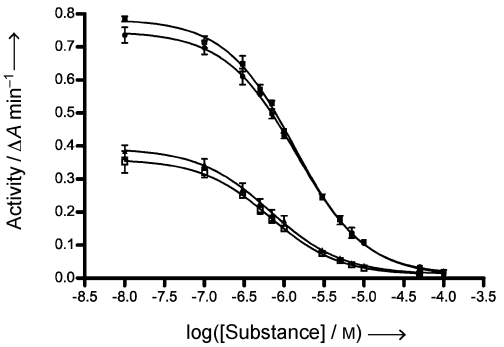

Figure 2. Dose–response curves used for determining IC_{50} values of **(*R*)-6** and **(*S*)-6** for wild-type *h*AChE and *m*AChE (with the *m*AChE concentration adjusted to a lower maximum activity than the *h*AChE concentration, for clarity). The enzymatic activity is measured as the increase in absorbance (Δ*A*) at 412 nm over time as a result of the enzymatic hydrolysis of acetylthiocholine.[3] Means ±S.D. from triplicate dose response curves (goodness of fit, $R^2 > 0.99$). Dose–response curves from the top: **(*R*)-6** *h*AChE (■), **(*S*)-6** *h*AChE (●), **(*S*)-6** *m*AChE (▲), **(*R*)-6** *m*AChE (□).

[*] L. Berg, M. S. Niemiec, Dr. C. D. Andersson, Prof. Dr. P. Wittung-Stafshede, Dr. A. Linusson
Department of Chemistry, Umeå University
90187 Umeå (Sweden)
L. Berg, Dr. C. D. Andersson, Dr. A. Linusson
Computational Life Science Cluster (CLiC), Umeå University
90187 Umeå (Sweden)
E-mail: anna.linusson@chem.umu.se
Dr. W. Qian
Laboratories for Chemical Biology Umeå
Chemical Biology Consortium Sweden
Department of Chemistry, Umeå University
90187 Umeå (Sweden)
Dr. F. Ekström
Swedish Defence Research Agency, CBRN Defence and Security
90182 Umeå (Sweden)
E-mail: fredrik.ekstrom@foi.se

[**] Acknowledgement is made to the Swedish Research Council and Umeå University for financial support. We thank Dr. D. Jansson (Swedish Defence Research Agency) for assistance with the chiral HPLC, Dr. M. Thunnissen (MAX-lab) for assistance during X-ray data collection, and HPC2N (High Performance Computing Center North) for HPC resources and technical support.

Supporting information for this article is available on the WWW under http://dx.doi.org/10.1002/anie.201205113.

© 2012 Wiley-VCH Verlag GmbH & Co. KGaA, Weinheim

Table 1: IC_{50} values and thermodynamic parameters for the binding of **(*R*)-6** and **(*S*)-6** to *Mus musculus* and *Homo sapiens* AChE.[3]

Species	Ligand	IC_{50}[a] [μM]	K_D [μM]	ΔG [kcal mol^{-1}]	ΔH [kcal mol^{-1}]	ΔS [cal mol^{-1} K^{-1}]	$-T\Delta S$ [kcal mol^{-1}]
Mus musculus	**(*R*)-6**	0.7	0.9	−8.1	−5.6	8.5	−2.5
Mus musculus	**(*S*)-6**	0.7	1.3	−7.9	−7.5	1.4	−0.4
Homo sapiens	**(*R*)-6**	1.3	1.7[b]	−7.8	−7.4[b]	1.5[b]	−0.4
Homo sapiens	**(*S*)-6**	1.4	2.2[b]	−7.7	−11.3[b]	−12.1[b]	3.6

[a] Mean values from triplicate dose response curves. [b] Mean values from two ITC experiments.

of enantiomers binding to AChE have indicated that the binding site exhibits a stereochemical preference.[4] To further investigate the binding properties, we determined the thermodynamic binding profiles by using isothermal titration calorimetry (ITC). The results of the ITC experiments confirm that the enantiomers have similar binding strength to both *m*AChE and *h*AChE (Table 1). However, the enthalpic and entropic contributions to the two enantiomers' free energy of binding (ΔG) differ (Table 1). **(*S*)-6** has a more favorable binding enthalpy for both *m*AChE and *h*AChE, but the entropic contribution is more pronounced for **(*R*)-6**, thus giving them similar ΔG values. These observations are in agreement with the entropy–enthalpy compensation phenomenon reported for protein–ligand complexation.[5] Notably, here such compensation is observed for enantiomers with similar ligand flexibility and desolvation.

To elucidate the structural basis of the difference in the enantiomers' binding properties, we determined the X-ray crystal structures of the complexes **(*R*)-6**/*m*AChE and **(*S*)-6**/*m*AChE at resolutions of 2.5 and 2.25 Å, respectively (Figure 3).[3,6] The electron density maps indicate that the two enantiomers coordinate to the PAS in similar conformations, in accordance with the previously published structure.[1] The data show that the complexes **(*R*)-6**/*m*AChE and **(*S*)-6**/*m*AChE differ primarily in terms of their conformations in the CAS (Figure 3).

The *N*-ethyl pyrrolidine moieties of the inhibitors extend towards Trp86 at the bottom of the active-site gorge, in conformations that are specific for each enantiomer. It is not possible to distinguish between the two tetrahedral configurations of the amine nitrogen from the electron density map of the complex with **(*R*)-6**, and so one major and one minor conformer were included in the final structure (A-**(*R*)-6** and B-**(*R*)-6**, Figure 3).[7] In both cases the *N*-ethyl substituent of **(*R*)-6** is directed toward residues Gly121, Gly122, Tyr124, and Phe297. In contrast, the *N*-ethyl substituent of **(*S*)-6** occupies a pocket formed by the aromatic rings of Tyr337, Phe338, and Tyr341 (Figure 3b). The complexes formed between the two enantiomers and *m*AChE also differ with respect to the conformation of Tyr337. In the **(*R*)-6**/*m*AChE complex, the side chain of Tyr337 was refined in two conformers of similar occupancy (conformers A and B),[8] whereas only one (which was equivalent to the A conformer) was observed for **(*S*)-6**/*m*AChE (Figure 3b). In the B conformer, Tyr337 is directed toward Phe338, closing off the pocket occupied by the *N*-ethyl substituent of **(*S*)-6**. The A conformer of Tyr337 is common in crystal structures of AChE, while the B conformer has been previously observed in only a few structures.[1,9] Taken together, there are four conformers of the **(*R*)-6**/*m*AChE complex to be considered: A and B conformers with respect to Tyr337 and also A and B conformers with respect to the configuration of the pyrrolidine nitrogen of the ligand. In contrast, there is only one conformer of the **(*S*)-6**/*m*AChE complex, as we do not observe any conformational mobility of Tyr337 and/or the ligand.

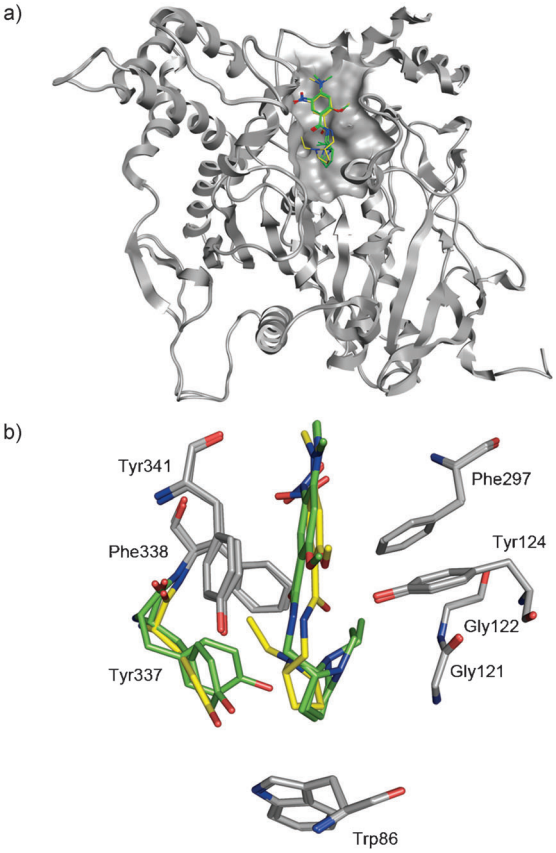

Figure 3. Overlay of the **(*R*)-6**/*m*AChE and **(*S*)-6**/*m*AChE crystal structures, showing the binding conformations of the two enantiomers a) in the binding cavity of *m*AChE and b) using a stick model and a subset of the adjacent amino acids. The carbon atoms of **(*S*)-6** are shown in yellow, while those of the two conformers A/B-**(*R*)-6** are shown in green. A and B conformers of residue Tyr337 in the **(*R*)-6**/*m*AChE complex are shown green, while Tyr337 in the **(*S*)-6**/*m*AChE complex is shown in yellow.

Noncovalent interactions in the crystal structures were then explored by using quantum mechanics.[3] More specifically, the geometries of reduced all-atom systems were optimized using density functional theory (DFT) with the M06-2X hybrid functional.[10] The electrostatic potentials were mapped on the calculated electron density surfaces and close interaction points were identified and analyzed.[11] The conformations of **(*S*)-6** and **(*R*)-6** appear to be stabilized in the CAS by a number of noncovalent interactions

 © 2012 Wiley-VCH Verlag GmbH & Co. KGaA, Weinheim

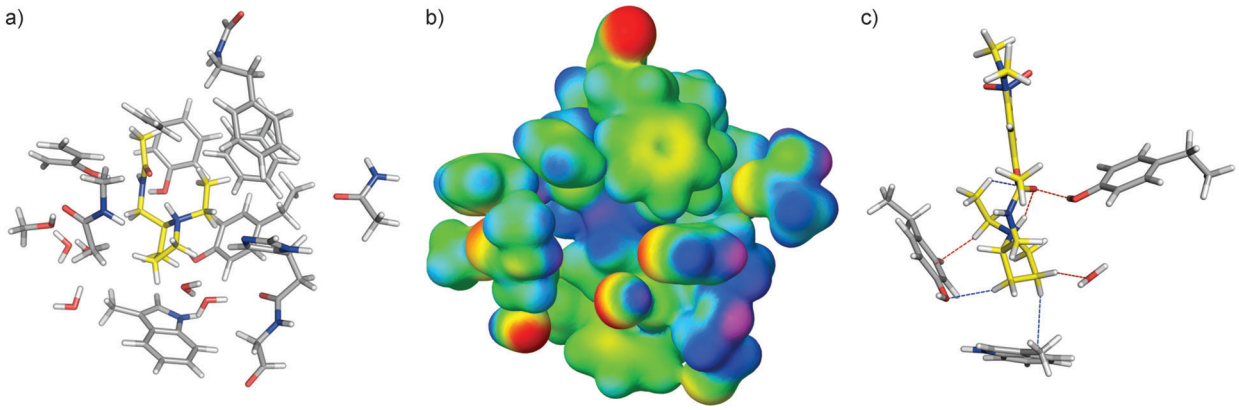

Figure 4. Identification of noncovalent interactions in the **(*S*)-6**/*m*AChE complex. a) Geometries of reduced all-atom systems (see text for modeling details), with ligand carbon atoms colored in yellow. b) Electrostatic potential mapped on the calculated electron density surface visualized by a spectrum from red (electron-rich) through orange, yellow, green, and blue to purple (electron-poor). c) Geometry-optimized structures shown using stick models with close interaction points highlighted by dashed lines. Residues Trp86, Tyr124 (right), Tyr337 (left), and water molecule W2211 are shown. Atoms of the ligand and Tyr124 that were not included in the DFT calculations have been added for clarity. Red and blue dashed lines indicate hydrogen bonds and van der Waals or electrostatic interactions, respectively.

(Figures 4 and 5),[3] including van der Waals and electrostatic interactions as well as both classical and nonclassical (here of CH···Y type) hydrogen bonds. Hydrogen bonds[12] of the CH···Y type (where Y represents for example arene or oxygen) are common in biological systems, and their role and importance have been widely discussed.[13] The geometry optimizations of the all-atom systems using M06-2X clearly resulted in a fine-tuning of the hydrogen-bond orientations in terms of both distances and angles compared to the crystal structures with added hydrogen atoms using molecular mechanics.

In the case of the **(*R*)-6**/*m*AChE complex, specific interaction patterns were established for each of the four systems based on the different conformers identified from the crystal structures. Note that the DFT geometry optimizations converged to similar conformations (within experimental error) of both conformers of the ligand and Tyr337.[3] This result supports the anticipated stability of the four geometries (Figure 5). The *N*-ethyl pyrrolidine group of **(*R*)-6** interacts with Tyr337, Trp86, Tyr124, and a water molecule through hydrogen bonds and/or electrostatic and van der Waals interactions in all four conformations. In the A-**(*R*)-6**-ATyr337 model, an internal hydrogen bond between the amide oxygen atom and the amine group of the pyrrolidine ring was observed (Figure 5a). In addition, three hydrogen bonds of the CH···O type were observed between the *N*-ethyl pyrrolidine group and both hydroxy groups of Tyr124 and Tyr337 and a water molecule. Van der Waals interactions with Trp86 were also observed (see Figure 5b–d for the interaction patterns of other conformers). We propose that the entropy change for the binding of **(*R*)-6** is more favorable than that for the binding of **(*S*)-6**, because in the former case, the ligand and protein can form attractive interaction patterns that allow an ensemble of multiple conformations, thus suggesting a greater degree of flexibility. However, it should be noted that the experimental X-ray data do not allow for detailed water analysis to elucidate solvation/desolvation effects. The importance of conformational entropy has been highlighted

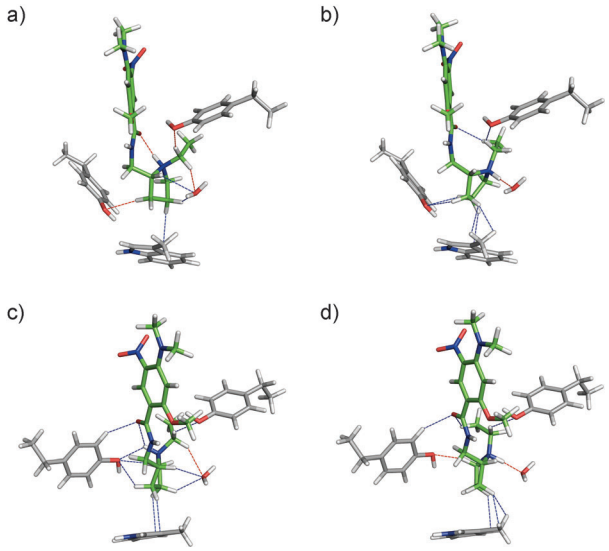

Figure 5. Noncovalent interactions in CAS between **(*R*)-6** and *m*AChE. Geometry-optimized structures are shown using stick models (ligand carbon atoms colored green) with close interaction points highlighted by dashed lines. (a) and (b) show the complexes featuring the A conformer of Tyr337 and the two alternative configurations of the amine (i.e. A-**(*R*)-6**-ATyr337 and B-**(*R*)-6**-ATyr337), while (c) and (d) show the B conformer of Tyr337 and the corresponding two configurations of the amine (A-**(*R*)-6**-BTyr337 and B-**(*R*)-6**-BTyr337). Residues Trp86, Tyr124 (right), Tyr337 (left), and water molecule W2126 are shown. Atoms of the ligand and Tyr124 that were not included in the DFT calculations have been added for clarity. Red and blue dashed lines indicate hydrogen bonds and van der Waals or electrostatic interactions, respectively.

in several recent studies,[5,14] which have shown cases where ligand preorganization by conformational restriction lead to entropic penalties in protein–ligand complex formation (these entropic penalties are contrary to previous expectations).[14a,b] A possible explanation is that the reduced flexibility of the ligand limits the conformational freedom of the formed complex. Both **(*R*)-6** and the protein examined in

 © 2012 Wiley-VCH Verlag GmbH & Co. KGaA, Weinheim

the present study can adopt different conformers that are stabilized by several relatively weak interactions. The net result is that the binding of **(*R*)-6** to *m*AChE is more entropically favorable than that of **(*S*)-6.**

The stabilizing interactions between the single conformation of **(*S*)-6** and the CAS are similar to those observed for **(*R*)-6** (Figure 4c). The amide oxygen atom forms both an internal hydrogen bond to the protonated amine of the pyrrolidine ring and a hydrogen bond with the hydroxy group of Tyr124. **(*S*)-6** also forms interactions with Trp86 and CH···O type hydrogen bonds with a water molecule. The positioning of the *N*-ethyl group between residues Tyr337 and Phe338 is stabilized by the internal hydrogen bond (Figure 3b). Geometry optimization of the system derived from the **(*S*)-6**/*m*AChE complex revealed the presence of an NCH···arene hydrogen bond between the aromatic ring of Tyr337 and one of the hydrogen atoms on the methylene group α to the nitrogen atom of the pyrrolidine ring (Figure 6). The distance between the methylene hydrogen atom and the plane of the

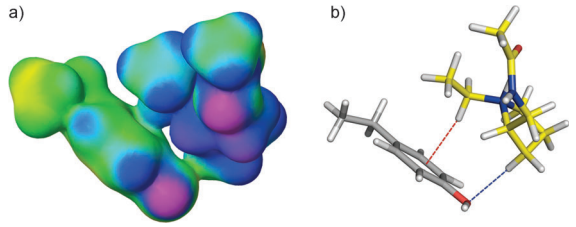

Figure 6. Detailed illustration of the interaction between Tyr337 of *m*AChE and the *N*-ethyl pyrrolidine group of **(*S*)-6**. a) The electrostatic potential mapped on the calculated electron density surface visualized by a spectrum from red (electron-rich) through orange, yellow, green, and blue to purple (electron-poor). b) Reduced stick model with close interactions indicated with dashed lines. The CH···arene hydrogen bond is highlighted in red.

arene's π system was 2.5 Å and the C–H–π plane angle was 165°. We suggest that this hydrogen bond between the activated C–H group and the aromatic ring of Tyr337 is the primary reason for **(*S*)-6** having a greater enthalpy of binding than its enantiomer. CH···arene interactions typically have energies of approximately 1.5–2.5 kcal mol^{-1}.[15] The mean CH/π plane distance for CH···arene hydrogen bonds in small organic molecules is 2.5–2.8 Å, and the mean C–H–π plane angle is 148–157°, depending on the strength of the proton donor involved.[15a,16] The closer the angle is to 180°, the stronger the interaction and the shorter the distance.[12] CH···arene interactions have also been detected in protein–ligand complexes,[13b,17] and their potential importance for ligand binding in AChE has been previously considered.[18] Here, we have identified a hydrogen bond between a C–H group in **(*S*)-6** and a tyrosine in *m*AChE; this hydrogen bond may explain the greater enthalpy upon complexation of **(*S*)-6**, relative to its enantiomer.

In this study we have shown that two enantiomers have similar binding affinities for AChE while differing in their thermodynamic profiles. By combining crystallography and computational chemistry, we were able to rationalize the observed entropy–enthalpy compensation. Analyses of the noncovalent interactions revealed that nonclassical hydrogen bonds of the CH···O and CH···arene types have a major influence on the enantiomers' binding properties. We believe that the identification and characterization of nonclassical hydrogen bonds will play increasingly important roles in elucidating the formation of protein–ligand complexes generally, and interactions involving AChE in particular.

Received: June 29, 2012
Revised: October 12, 2012
Published online: November 19, 2012

Keywords: aromatic interactions · density functional calculations · molecular recognition · nonclassical hydrogen bonds · stereoselectivity

[1] L. Berg, C. D. Andersson, E. Artursson, A. Hörnberg, A.-K. Tunemalm, A. Linusson, F. Ekström, *PLoS ONE* **2011**, *6*, e26039.
[2] D. Renneberg, P. B. Dervan, *J. Am. Chem. Soc.* **2003**, *125*, 5707.
[3] For further details, see the Supporting Information.
[4] a) M. McKinney, J. H. Miller, F. Yamada, W. Tuckmantel, A. P. Kozikowski, *Eur. J. Pharmacol.* **1991**, *203*, 303; b) A. Saxena, N. Qian, I. M. Kovach, A. P. Kozikowski, Y. P. Pang, D. C. Vellom, Z. Radic, D. Quinn, P. Taylor, B. P. Doctor, *Protein Sci.* **1994**, *3*, 1770; c) P. Camps, R. El Achab, J. Morral, D. Muñoz-Torrero, A. Badia, J. E. Baños, N. M. Vivas, X. Barril, M. Orozco, F. J. Luque, *J. Med. Chem.* **2000**, *43*, 4657.
[5] C. H. Reynolds, M. K. Holloway, *ACS Med. Chem. Lett.* **2011**, *2*, 433.
[6] The crystal structures have been deposited in the Protein Data Bank (PDB), PDB codes 4ARA and 4ARB.
[7] The maximal atom deviation of the two conformers is 0.82 Å and the apparent occupancies are 0.89 and 0.11.
[8] The maximal atom deviation of the two Tyr337 conformers is 3.99 Å and the apparent occupancies are 0.44 and 0.56.
[9] a) Y. Bourne, H. C. Kolb, Z. Radic, K. B. Sharpless, P. Taylor, P. Marchot, *Proc. Natl. Acad. Sci. USA* **2004**, *101*, 1449; b) F. Ekström, A. Hörnberg, E. Artursson, L. G. Hammarström, G. Schneider, Y. P. Pang, *PLoS ONE* **2009**, *4*, e5957.
[10] Y. Zhao, D. Truhlar, *Theor. Chem. Acc.* **2008**, *120*, 215.
[11] The noncovalent interactions were determined by visual inspection of the electrostatic potential mapped on the calculated electron density at an isovalue of 0.007 electrons/Bohr^3, as well as distances and angles. Further details and all close contacts in the complexes can be found in the Supporting Information.
[12] a) E. Arunan, G. R. Desiraju, R. A. Klein, J. Sadlej, S. Scheiner, I. Alkorta, D. C. Clary, R. H. Crabtree, J. J. Dannenberg, P. Hobza, H. G. Kjaergaard, A. C. Legon, B. Mennucci, D. J. Nesbitt, *Pure Appl. Chem.* **2011**, *83*, 1619; b) E. Arunan, G. R. Desiraju, R. A. Klein, J. Sadlej, S. Scheiner, I. Alkorta, D. C. Clary, R. H. Crabtree, J. J. Dannenberg, P. Hobza, H. G. Kjaergaard, A. C. Legon, B. Mennucci, D. J. Nesbitt, *Pure Appl. Chem.* **2011**, *83*, 1637.
[13] a) G. R. Desiraju, T. Steiner, *The weak hydrogen bond in structural chemistry and biology*, Oxford University Press, New York, **1999**; b) S. Sarkhel, G. R. Desiraju, *Proteins Struct. Funct. Bioinf.* **2004**, *54*, 247; c) G. R. Desiraju, *Chem. Commun.* **2005**, 2995; d) C. Bissantz, B. Kuhn, M. Stahl, *J. Med. Chem.* **2010**, *53*, 5061; e) P. Hobza, K. Muller-Dethlefs, *Non-covalent interactions. Theory and experiment*, The Royal Society of Chemistry, Cambridge, **2010**; f) W. A. Herrebout, M. A. Suhm, *Phys. Chem. Chem. Phys.* **2011**, *13*, 13858; g) S. Melandri, *Phys. Chem. Chem.*

 © 2012 Wiley-VCH Verlag GmbH & Co. KGaA, Weinheim

Phys. **2011**, *13*, 13901; h) S. Scheiner, *Phys. Chem. Chem. Phys.* **2011**, *13*, 13860.

[14] a) A. P. Benfield, M. G. Teresk, H. R. Plake, J. E. DeLorbe, L. E. Millspaugh, S. F. Martin, *Angew. Chem.* **2006**, *118*, 6984; *Angew. Chem. Int. Ed.* **2006**, *45*, 6830; b) J. E. DeLorbe, J. H. Clements, M. G. Teresk, A. P. Benfield, H. R. Plake, L. E. Millspaugh, S. F. Martin, *J. Am. Chem. Soc.* **2009**, *131*, 16758; c) B. Baum, L. Muley, M. Smolinski, A. Heine, D. Hangauer, G. Klebe, *J. Mol. Biol.* **2010**, *397*, 1042; d) C. Diehl, O. Engström, T. Delaine, M. Håkansson, S. Genheden, K. Modig, H. Leffler, U. Ryde, U. J. Nilsson, M. Akke, *J. Am. Chem. Soc.* **2010**, *132*, 14577; e) J. M. Ward, N. M. Gorenstein, J. Tian, S. F. Martin, C. B. Post, *J. Am. Chem. Soc.* **2010**, *132*, 11058.

[15] a) M. Nishio, *Phys. Chem. Chem. Phys.* **2011**, *13*, 13873; b) L. M. Salonen, M. Ellermann, F. Diederich, *Angew. Chem.* **2011**, *123*, 4908; *Angew. Chem. Int. Ed.* **2011**, *50*, 4808.

[16] O. Takahashi, Y. Kohno, S. Iwasaki, K. Saito, M. Iwaoka, S. Tomoda, Y. Umezawa, S. Tsuboyama, M. Nishio, *Bull. Chem. Soc. Jpn.* **2001**, *74*, 2421.

[17] a) T. Steiner, G. Koellner, *J. Mol. Biol.* **2001**, *305*, 535; b) M. Harigai, M. Kataoka, Y. Imamoto, *J. Am. Chem. Soc.* **2006**, *128*, 10646; c) S. K. Panigrahi, G. R. Desiraju, *Proteins Struct. Funct. Bioinf.* **2007**, *67*, 128.

[18] a) H. Dvir, H. L. Jiang, D. M. Wong, M. Harel, M. Chetrit, X. C. He, G. Y. Jin, G. L. Yu, X. C. Tang, I. Silman, D. L. Bai, J. L. Sussman, *Biochemistry* **2002**, *41*, 10810; b) G. Koellner, T. Steiner, C. B. Millard, I. Silman, J. L. Sussman, *J. Mol. Biol.* **2002**, *320*, 721.

 © 2012 Wiley-VCH Verlag GmbH & Co. KGaA, Weinheim